Effects of molecular charge density polarization on X(1) and X(2)

Seidler, T.; Stadnicka, K.; Champagne, B.

Published in:
Proceedings of SPIE

DOI:
10.1117/12.2027343

Publication date:
2013

Document Version
Publisher's PDF, also known as Version of record

Effects of molecular charge density polarization on $\chi^{(1)}$ and $\chi^{(2)}$: a computational study of 2-methyl-4-nitroaniline (MNA) and 4-(*N*,*N*-dimethylamino)-3-acetamidonitrobenzene (DAN)

T. Seidler[a,b,*,†], K. Stadnicka[a], B. Champagne[b,*]
[a]Faculty of Chemistry, Jagiellonian University, ul. Ingardena 3, 30-060 Cracow, Poland;
[b]Laboratoire de Chimie Théorique, UCPTS, University of Namur, rue de Bruxelles, 61, B-5000, Namur, Belgium
[†]seidler@chemia.uj.edu.pl

ABSTRACT

The linear and second-order nonlinear optical susceptibilities of the MNA and DAN organic molecular crystals have been determined using a computationally cheap method, the Rigorous Local Field Theory, which consists in estimating the bulk properties from 1°) the corresponding molecular responses, evaluated using quantum chemistry methods, as well as 2°) the local and dressing electric fields, evaluated using a classical electrostatic interaction scheme.

This study has highlighted several conditions for obtaining accurate theoretical results. First, the input molecular geometry should match the main features of the crystal structure. Then, the molecular properties should be evaluated at a correlated level since electron correlation effects are huge for the polarizability (α) and even more for the first hyperpolarizability (β). The recommended approach is to use static MP2 molecular responses together with the multiplicative scheme to describe frequency dispersion. The third important aspect is the impact of the chromophore electron density polarization due to surrounding molecules in the crystal lattice. This effect accounts for an enhancement of *ca.* 100-200% of β and thus influences strongly the calculated bulk $\chi^{(2)}$ tensor components.

Keywords: Non-linear optics, molecular crystals, MNA, DAN

1. INTRODUCTION

Organic molecular crystals constitute an important class of second-order nonlinear optical (NLO) materials[1,2]. Understanding these NLO responses together with designing new organic crystals with large NLO responses would benefit from their predictions using quantum mechanics approaches[3] but in many cases, the computational methods are still incapable of handling such large systems on the grounds of a full *ab initio* treatment. The most elaborate, and most accurate, methods consist in solving for the organic solids the Bethe-Salpeter or related equations, accounting for electron correlation effects. On the other hand, the current implementations of time-dependent density functional theory (TD-DFT) neglect the charge-transfer excitons as it does not describe correctly the electron-hole interactions so its use, even in the static limit, is controversial. In this view, methods that are based on the properties of the isolated constitutive molecules are still a very good while computationally cheap alternative.

In this contribution a computational study of two derivatives of *p*-nitroaniline is presented, namely, 2-methyl-4-nitroaniline (MNA) and 4-(*N*,*N*-dimethylamino)-3-acetamidonitrobenzene (DAN). In both cases, the introduction of substituents yields crystallization in noncentrosymmetric space groups: Ia[4] and $Pna2_1$[5], respectively, thus allowing the second-order nonlinearities. To evaluate the linear and second-order nonlinear optical susceptibilities, $\chi^{(1)}$ and $\chi^{(2)}$, the Rigorous Local Field Theory (RLFT) due to Hurst & Munn[6] is applied here and the results are compared with experiment. This approach consists in estimating the macroscopic properties from the corresponding molecular responses by accounting for both the local and dressing electric fields. It is shown that the uniform dipole (dressing) electric field, originating from the surrounding and polarizing the NLO-phore electron density should be accounted for in order to reproduce the experimental linear susceptibilities with good accuracy. The corresponding theoretical refractive indices are then used to determine the directions of types I and II phase-matching. In the last step, the full second-order susceptibility tensor is projected along these directions and compared with the experimental results. The effect of the electron correlation in the calculations of response for isolated molecules is also discussed.

Optical Processes in Organic Materials and Nanostructures II,
edited by Manfred Eich, Jean-Michel Nunzi, Rachel Jakubiak, Proc. of SPIE
Vol. 8827, 88270Y · © 2013 SPIE · CCC code: 0277-786X/13/$18 · doi: 10.1117/12.2027343

2. COMPUTATIONAL METHODOLOGY

2.1 The electrostatic interaction scheme

The susceptibilities are measures of how matter responds to an external electric field. For molecules it is governed by the polarizability α and hyperpolarizability (β, γ,...) tensors. Up to second order, the total electric dipole moment reads

$$\underline{p} = \underline{p}_0 + \underline{\underline{\alpha}} \cdot \underline{F} + \frac{1}{2}\underline{\underline{\underline{\beta}}} : \underline{F}\,\underline{F} + \ldots \tag{1}$$

where F is the local electric field. Its macroscopic analogue is

$$\underline{P}/\varepsilon_0 = \underline{\underline{\chi}}^{(1)} \cdot \underline{E} + \underline{\underline{\underline{\chi}}}^{(2)} : \underline{E}\,\underline{E} + \ldots \tag{2}$$

where P is the induced macroscopic polarization, ε_0 is the electric permittivity of the vacuum, and E is the externally applied electric field. The correspondence between the microscopic and macroscopic properties demands relating the external (E) and local (F) electric fields. Considering the molecular induced dipole moments as sources of the polarizing field in an infinite crystal lattice one can write, using linear algebra, such relationships under the form[6]

$$\underline{F}_k = \underline{\underline{d}}_k \cdot \underline{E} \tag{3}$$

where $\underline{\underline{d}}_k$, the local field tensor for molecule or submolecule k, is defined, in the dipole approximation as

$$\underline{\underline{d}}_k(\omega) = \sum_{k'} \underline{\underline{D}}_{kk'}(\omega) = \sum_{k'} \left[\underline{\underline{1}} - \frac{1}{V\varepsilon_0} \underline{\underline{\alpha}}(\omega) \cdot \underline{\underline{L}} \right]^{-1}_{kk'} \tag{4}$$

$\underline{\underline{\alpha}}(\omega)$ is the block-diagonal supermatrix of the molecular polarizabilities and $\underline{\underline{L}}$ is the Lorentz factor tensor, and the summation is performed over all (sub)molecules in the unit cell. The local field tensor $\underline{\underline{d}}_k$ describes the screening of the external electric field by the polarizable molecular surrounding. Usually the molecules are too large and too complicated to be reduced to single "dipole moments" or "polarizabilities", so that the submolecular approach should be used[7]. The optimum and physically most reasonable choice for the submolecules in organic systems are the heavy (non-hydrogen) atoms - groups such as NH_n, CH_n, OH_n are almost isoelectronic so their contribution to the total molecular polarizability could be treated *ad hoc* as equal. In the literature[7,8] this choice is referred to as RLFTn where n is the number of heavy (non-hydrogen) atoms. Therefore, the working equations for obtaining the linear susceptibilities as well as the second-order nonlinear optical susceptibilities for second harmonic generation process (SHG) are[6]

$$\underline{\underline{\chi}}^{(1)}(-\omega;\omega) = \frac{1}{V\varepsilon_0} \sum_k \underline{\underline{\alpha}}_k(\omega) \cdot \underline{\underline{d}}_k(\omega) \tag{5}$$

$$\underline{\underline{\underline{\chi}}}^{(2)}(-2\omega;\omega,\omega) = \frac{1}{2V\varepsilon_0} \sum_k \underline{\underline{d}}_k^T(2\omega) \cdot \underline{\underline{\underline{\beta}}}_k : \underline{\underline{d}}_k(\omega)\,\underline{\underline{d}}_k(\omega) \tag{6}$$

Since the molecules in the present study are polar, when placed in a infinite periodic lattice they constitute a source of polarizing (dressing) electric field. This field was taken into account with the use of equation[8]

$$\underline{F}_k = \frac{1}{V\varepsilon_0} \sum_{k',k''} \underline{\underline{D}}_{kk'}(\omega = 0) \cdot \underline{\underline{L}}_{k'k''} \cdot \underline{p}_{k0} \tag{7}$$

This leads to a self-consistent cycle to determine the polarizing electric field (Figure 1). The permanent dipole moment used at every iteration of the procedure is the one obtained in the absence of the polarizing field. The charge density responds to the static electric field only *via* the dipole polarizability of the submolecules (Eq. 7). The calculations are considered as converged if the electric field between consecutive cycles does not change by more than 0.0001 a.u. (*ca.* 0.05 GV/m). Note that the experimentally reported d_{eff} quantity corresponds to half of χ_{eff} for the SHG process.

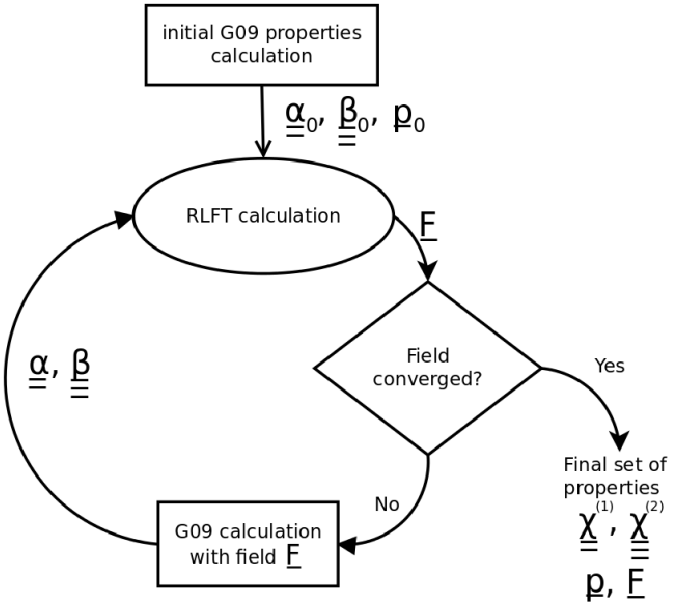

Fig. 1. Graphical scheme of the self-consistent field procedure within the RLFT method (G09 stands for Gaussian09[9] quantum chemistry package used for isolated molecule calculations).

2.2 Quantum chemistry methods

The chromophoe geometry was fully optimized using density functional theory (DFT) and in particular the B3LYP exchange-correlation functional as available in Gaussian09[9]. The 6-311++G(d,p) atomic basis set was employed. In the case of DAN, as the optimized geometry differs greatly with respect to those in the crystal structure, the second one was also used. The only modification from X-ray diffraction data was the adjustment of the X-H bond lengths to the averaged neutron diffraction data[10]: 1.083 Å for aromatic C-H, 1.077 Å for CH_3 group, and 1.030 Å for N-H.

The static (ω=0) molecular properties were calculated using the Coupled Perturbed Hartree-Fock (CPHF) method and Coupled Perturbed Kohn-Sham (CPKS) method with the B3LYP functional and the 6-311++G(3df,3pd) basis set. In order to assess the impact of electron correlation, the MP2/6-311++G(d,p) method in combination with the finite field scheme was also used to calculate the static (hyper)polarizabilities. Dynamic properties were obtained using the time-dependent Hartree-Fock and TD-DFT methods. These were combined with the MP2 static values within the multiplicative approach to estimate dynamic MP2 polarizabilities :

$$\alpha_{ij}^{MP2}(\omega) = \alpha_{ij}^{MP2}(\omega=0)\frac{\alpha_{ij}^{TDDFT/B3LYP}(\omega)}{\alpha_{ij}^{CPKS/B3LYP}(\omega=0)} \tag{8}$$

This multiplicative correction was performed in the eigenbasis of the static MP2 polarizability tensor. The dynamic MP2 first hyperpolarizabilities tensor elements were obtained using the analogous expression

$$\beta_{ijk}^{MP2}(\omega) = \beta_{ijk}^{MP2}(\omega=0)\frac{\beta_{tot}^{TDDFT/B3LYP}(\omega)}{\beta_{tot}^{CPKS/B3LYP}(\omega=0)} \tag{9}$$

where

$$\beta_{tot} = \frac{1}{5}\left[\sum_{i,j}\left(\beta_{ijj}+\beta_{jij}+\beta_{jji}\right)^2\right]^{1/2} \tag{10}$$

This simple scheme does not account for the breaking of Kleinman's symmetry for the hyperpolarizability tensor, however, it is introduced in the bulk properties via the frequency dispersion of the polarizability (Eq. 6).

3. RESULTS AND DISCUSSION

3.1 2-methyl-4-nitroaniline (MNA)

2-methyl-4-nitroaniline crystallizes in the monoclinic system, space group Ia, with 4 molecules in the unit cell[4]. The crystal symmetry fixes only the *y* indicatrix axis as parallel to the *b* crystallographic direction. The angle between the projection of the molecular charge-transfer (CT) axis on the (010) crystallographic plane and the *a* crystallographic axis is *ca.* 26° (Figure 2. left) and so it defines the relative position of the remaining *x*, *z* indicatrix axes with respect to the crystallographic frame. *x* is approximately parallel to the CT axis, which justifies the highest value of the n_x refractive index. These simple considerations are in full agreement with all the RLFT calculations.

The variation of the dipole moment upon accounting for the dressing electric field, as obtained from B3LYP and MP2 molecular responses, is presented in Table 1 and schematically shown in Figure 2 (right). A characteristic and common feature to all the calculations – in fact, for both systems – is that the electric field is aligned almost parallel to the molecular dipole moment and induces an enhancement of the molecular dipole moment of the order of 55-65%. Then, the largest (in-plane) polarizability component is mostly affected, the change of the isotropic polarizability is of the order of 5.5% while more drastic changes are observed for the first hyperpolarizability: 80-100%.

Table 1. MNA dipole moment p components (in Debye), electric field F components (in GV/m), static isotropic polarizability $\alpha_{iso} = 1/3\ (\alpha_{xx} + \alpha_{yy} + \alpha_{zz})$ (a.u.) and norm of the vectorial hyperpolarizability β_{tot} (a.u.) before and after accounting for the dressing electric field.

Method	cycle	p_x	p_y	p_z	F_x	F_y	F_z	α	β_t
B3LYP	0-th	7.37	-0.90	0.62	4.61	-0.15	0.47	119.9	901
	last	12.16	-1.16	0.75	4.97	0.17	0.42	126.7	1605
MP2	0-th	6.65	-0.79	0.68	3.93	-0.11	0.67	111.6	961
	final	10.29	-0.96	0.86	4.19	-0.12	0.63	117.8	1915

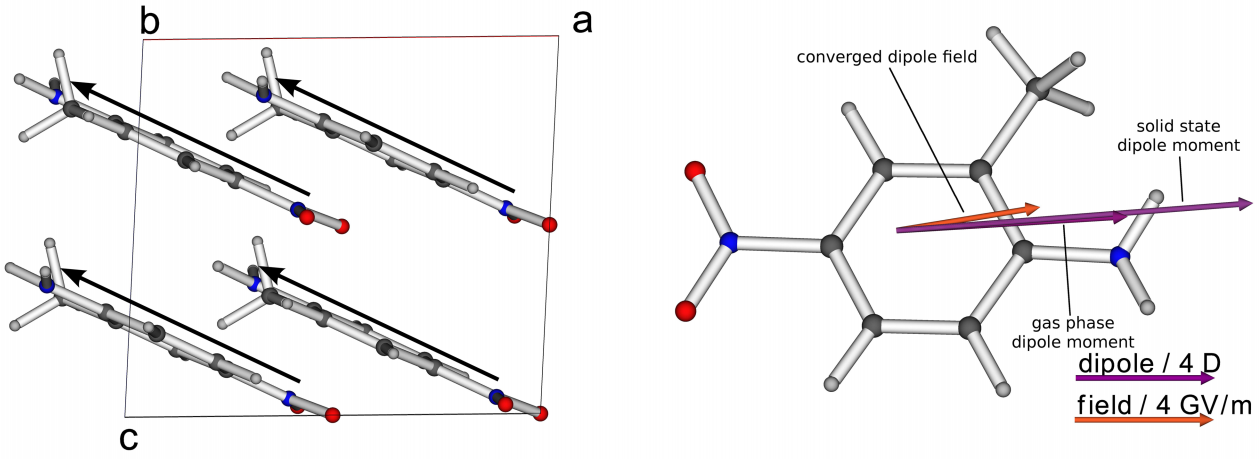

Fig. 2. (010) plane projection of MNA crystal structure together with the approximate charge-transfer direction on every molecule (left) and illustration of the molecular dipole moment enhancement in the MNA crystal phase obtained from the iterative procedure described by Eq. 7 (right). The molecular properties are calculated at the MP2 level. The dressing electric field is also represented.

$\chi^{(1)}$ and $\chi^{(2)}$ are then evaluated following Eqs. (5)-(6). The effect of the polarizing electric field on the static bulk properties is presented in Table 2. The influence of the electron correlation, estimated by the difference between the results of MP2 calculations with respect to HF results shows that the latter method underestimates n_x and n_y, while for the smallest one, n_z, it gives a slight overestimation. For the dynamic properties the discrepancy is even larger since the TDHF method underestimates the absorption frequencies. On the other hand, a combination of static MP2 properties with B3LYP frequency dispersion according to Eq. 8 and 9 leads to a very good agreement with experiment[11] while the *pure* B3LYP method slightly overestimates the refractive indices. However, the greatest challenge appears to be n_x of which the strong frequency dispersion is not fully reproduced. Theoretical and experimental dispersions of the refractive indices are displayed in Figure 3.

The experimental values of the $\chi^{(2)}$ tensor components were published in several papers[12-14]. Taking the reference values of d_{11}=0.30(2) pm/V for α-quartz[15] and d_{33}=27 pm/V for $LiNbO_3$[16], we concluded that $\chi^{(2)}_{111}$ is of the order of 300 pm/V at 1064 nm and d_{12}=22.5 pm/V. The calculated tensor values, presented in Table 2 are in reasonably good agreement with experiment providing the polarizing field is taken into consideration. The dispersion of $\chi^{(2)}_{111}$ tensor component is shown in Figure 4. In the case of $\chi^{(2)}$ the polarizing field effect accounts for a 100% to even 200% increase of the calculated property. The sign of the $\chi^{(2)}$ tensor elements is connected to the absolute polarity of the structure and is difficult to be determined experimentally. The calculated ratio $\chi^{(2)}_{111}/\chi^{(2)}_{122}$ amounts to *ca.* 10 (as determined from MP2 method) is larger than the one reported experimentally (*ca.* 4), however only one experimental paper reports the value of this ratio[14].

Table 2. Static bulk properties of MNA obtained with different approaches.

Method	λ / nm	n_x	n_y	n_z	$\chi^{(2)}_{111}$ pm/V	$\chi^{(2)}_{122}$	$\chi^{(2)}_{212}$
HF no field	∞	1.799	1.675	1.443	-25.1	-0.1	
	1064	1.817	1.685	1.446	-36.5	-0.1	-1.0
HF field conv.	∞	1.857	1.676	1.440	-49.4	-2.7	
	1064	1.883	1.687	1.444	-78.2	-3.6	-5.5
B3LYP no field	∞	1.943	1.724	1.461	-55.9	-3.3	
	1064	1.982	1.738	1.465	-118.7	-6.5	-9.2
B3LYP field conv.	∞	2.069	1.733	1.456	-106.9	-8.1	
	1064	2.139	1.751	1.459	-317.3	-18.0	-24.0
MP2 no field	∞	1.850	1.697	1.425	-49.2	-5.2	
	1064	1.884	1.709	1.429	-105.6	-11.0	-10.5
MP2 field conv.	∞	1.964	1.710	1.421	-114.2	-11.6	
	1064	2.025	1.725	1.425	-327.1	-31.4	-28.1
experiment	∞	1.953[11]	1.719[11]	1.436[11]			
	1064	2.063[11]	1.732[11]	1.439[11]	300(75)[12-14]	45[14]	

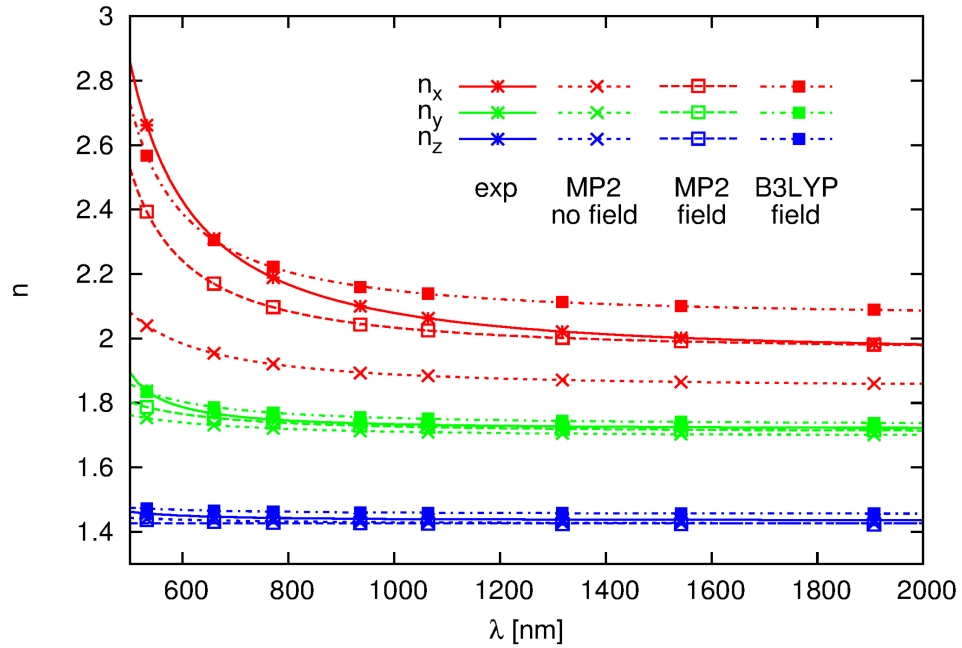

Fig. 3. Experimental[11] and theoretical dispersion of the refractive indices of MNA.

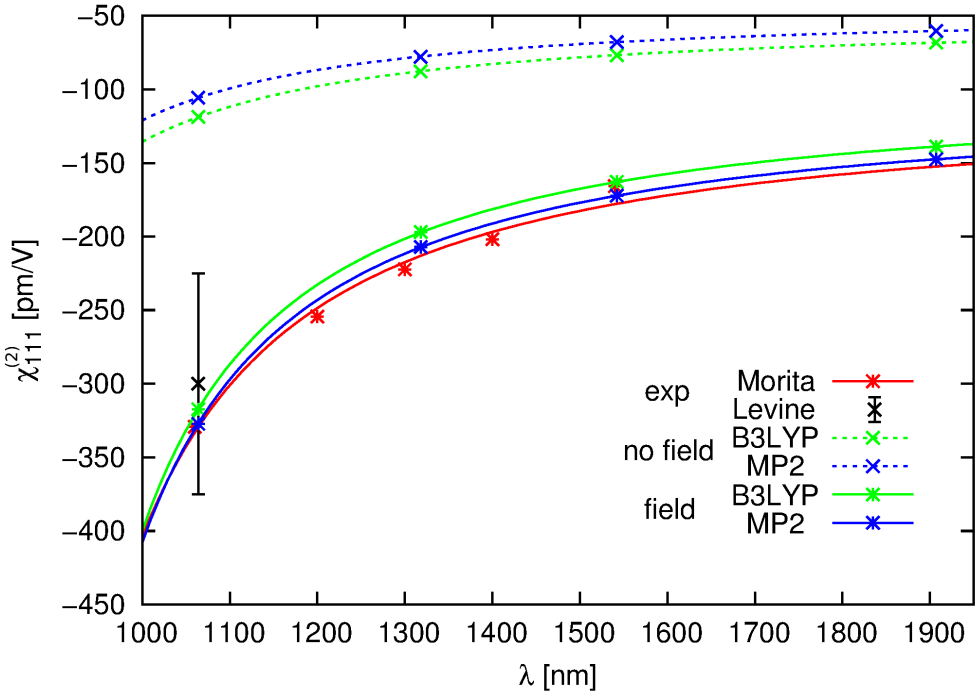

Fig. 4. Experimental[12,13] and theoretical dispersion of $\chi^{(2)}_{111}$ of MNA.

3.2 4-(*N*,*N*-dimethylamino)-3-acetamidonitrobenzene (DAN)

DAN crystallizes also in monoclinic system in space group $P2_1$ with two molecules per unit cell[5]. The structure is mainly stabilized by a network of hydrogen bonds between the acetamido substituents. Molecular geometry optimization disregards these interactions and results in flattening of the acetamido group with respect to the aromatic ring. This is schematically shown in Figure 5. Besides this, the bond length alternation[17] (BLA) is also affected by the structure flattening: it drops down from 0.036 Å to only 0.006 Å. In the case of DAN, the angle between the CT projection on the (010) plane and the *c* crystallographic axis is *ca.* 35° (Figure 6 left). The *z* indicatrix axis defined approximately along the CT direction justifies the largest refractive index to be n_z. This experimental value[18] is fully consistent with the theoretical results.

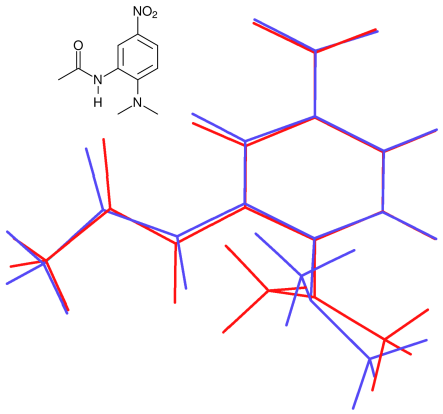

Fig. 5. Sketch of the DAN molecular geometry (red – modified geometry from X-ray diffraction crystal structure, blue – optimized geometry at the B3LYP level).

The evolution of the dipole moment, of the polarizing electric field, and of selected static molecular properties is presented in Table 3 and Figure 6 (right). Again the inclusion of the polarizing field leads to significant enhancements of the properties. The geometry effect is more pronounced in case of the MP2 method.

Table 3. DAN dipole moment p components (in Debye), electric field F components (in GV/m), static isotropic polarizability α (a.u.) and norm of vectorial hyperpolarizability β_{tot} (a.u.) (I: single molecule optimized geometry, II: modified crystal geometry II).

Method	cycle	p_x	p_y	p_z	F_x	F_y	F_z	α	β_t
B3LYP I	0-th	-8.00	-4.68	-0.61	-2.83	-2.80	-1.49	170.0	759
	last	-11.43	-7.56	-1.39	-2.93	-2.88	-1.51	175.3	1914
B3LYP II	0-th	-8.43	-4.96	-2.11	-3.06	-3.02	-3.37	170.4	1142
	last	-12.67	-8.22	-3.80	-3.24	-3.16	-3.40	178.2	2141
MP2 I	0-th	-7.40	-4.44	-0.56	-2.50	-2.55	-1.30	158.5	484
	last	-9.97	-6.84	-1.21	-2.54	-2.58	-1.31	161.3	1094
MP2 II	0-th	-7.73	-4.62	-2.02	-2.69	-2.70	-3.08	159.7	1079
	last	-11.14	-7.39	-3.52	-2.84	-2.82	-3.12	168.0	2468

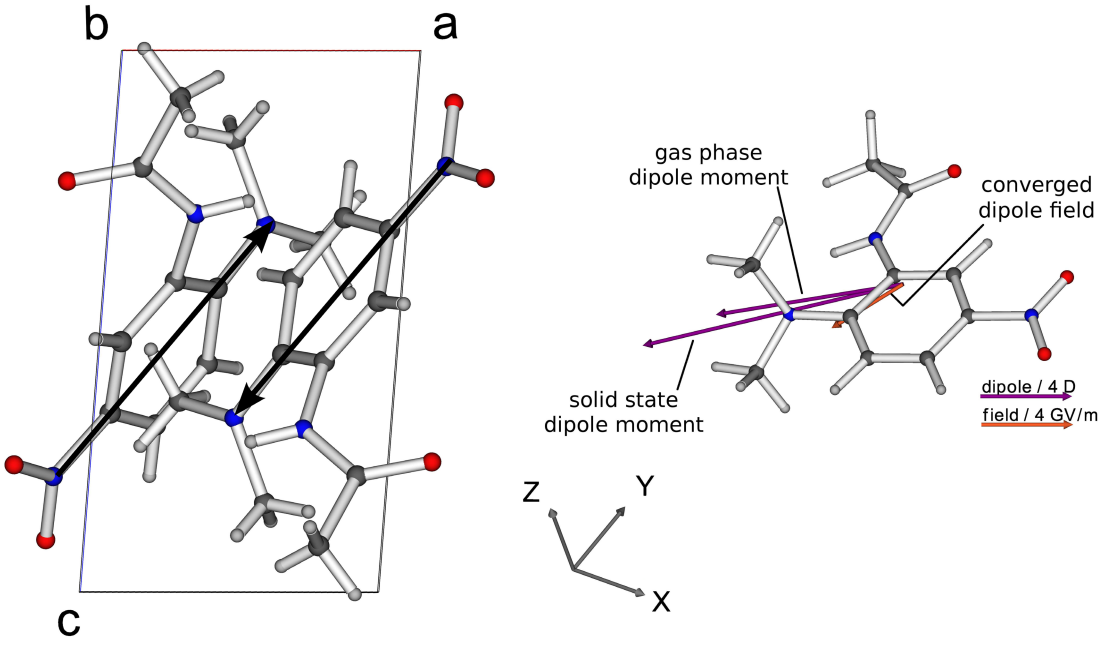

Fig. 6. (010) plane projection of DAN crystal structure together with the approximate charge-transfer direction on every molecule (left) and illustration of the molecular dipole moment enhancement in the DAN crystal phase obtained from the iterative procedure described by Eq. 7 (right). The dressing electric field is also represented.

The calculated static and dynamic (for λ=1064 nm) bulk properties are summarized in Table 4. A comparison between the theoretical and experimental refractive indices is shown in Figure 7. Using both MP2 and B3LYP molecular properties, it turns out that the bulk properties obtained using the optimized isolated molecule geometry can be severely underestimated with respect to experiment, in particular the n_z refractive index and the $\chi^{(2)}_{233}$ tensor component.

A comparison between the experimentally-determined and the calculated phase matching configurations of types I and II are presented in Figure. 8. The experimental quantities and those predicted theoretically overlap quite well for type I, which is of greater practical importance. A slight underestimation of the angle range results from the small n_z overestimation and n_x, n_y underestimation. However, the calculated d_{eff} values match well the experiment.

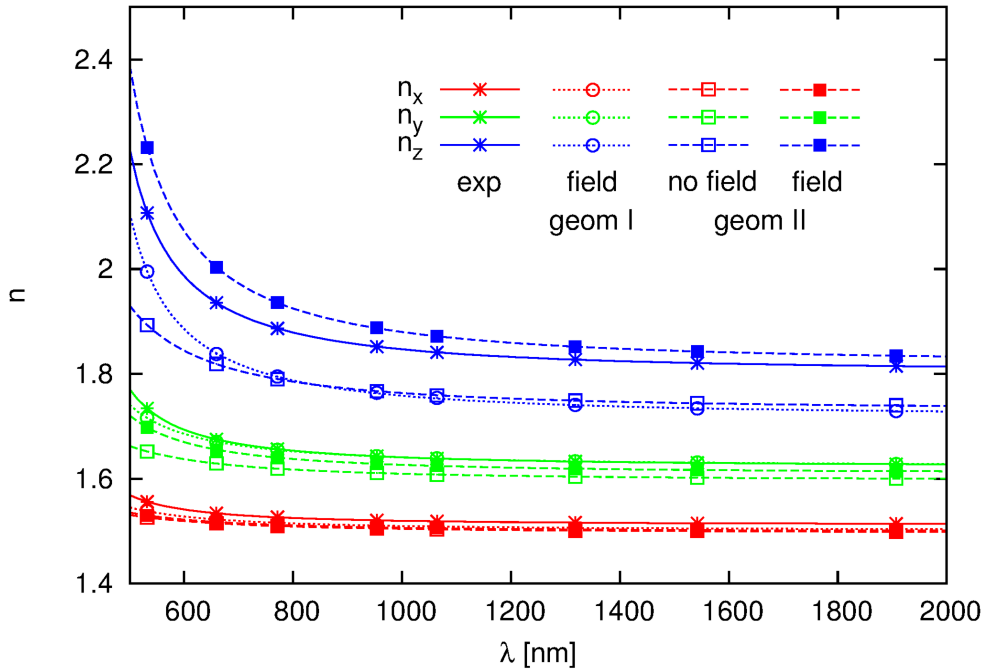

Fig. 7. Experimental[18] and theoretical dispersion of refractive indices of DAN obtained with MP2 method.

Table 4. Static bulk properties of DAN obtained with different approaches.

Method	λ / nm	n_x	n_y	n_z	$\chi^{\square\square\square}_{\square\square\square}$	$\chi^{\square\square\square}_{\square\square\square}$	$\chi^{\square\square\square}_{222}$
B3LYP I no field	∞	1.539	1.661	1.770	-11.0		2.6
	1064	1.545	1.676	1.793	-27.7	-24.9	2.8
B3LYP II no field	∞	1.526	1.633	1.810	-17.7		4.1
	1064	1.533	1.647	1.841	-41.4	-39.0	4.6
B3LYP II field conv.	∞	1.526	1.642	1.903	-31.6		1.2
	1064	1.532	1.661	1.960	-120.3	-108.9	-4.8
MP2 I no field	∞	1.502	1.618	1.690	-4.2		0.9
	1064	1.509	1.632	1.710	-10.5	-9.4	-2.3
MP2 II no field	∞	1.497	1.597	1.731	-13.0		2.1
	1064	1.503	1.608	1.759	-30.4	-30.9	4.4
MP2 II field conv.	∞	1.499	1.610	1.820	-30.3		0.2
	1064	1.506	1.625	1.872	-103.7	-106.4	-2.1
experiment[18]	1064	1.519	1.639	1.841	100(30)		10.4(2.0)

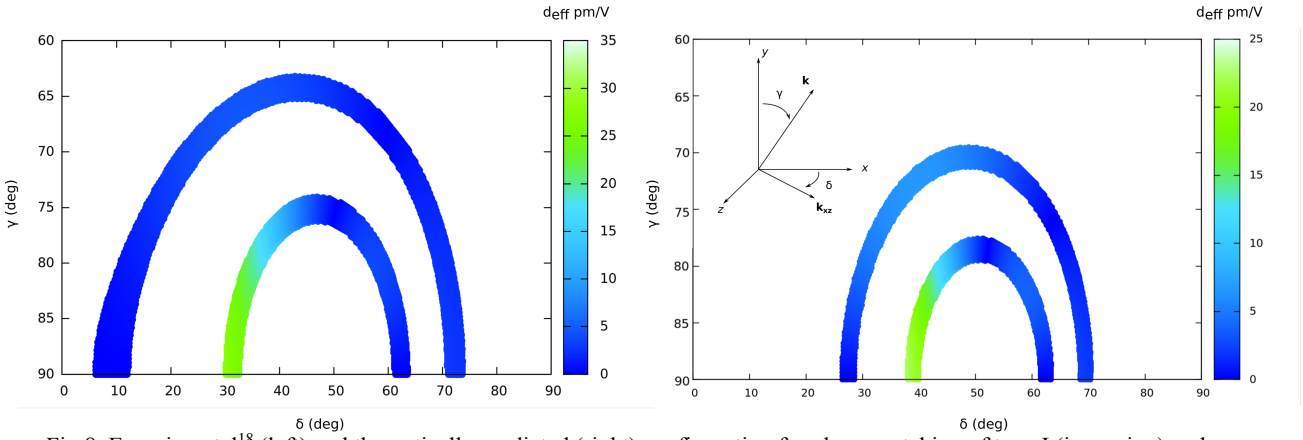

Fig 8. Experimental[18] (left) and theoretically predicted (right) configuration for phase matching of type I (inner ring) and type II (outer ring); the angles between the indicatrix axes (x,y,z) and the propagation (**k**) vector are defined on the right part of the Figure.

4. CONCLUSIONS

The current contribution gives a concise summary of the capabilities of the RLFT methodology to predict the linear and second-order nonlinear optical susceptibilities of organic molecular crystals. The study has highlighted several conditions for obtaining accurate theoretical results. First, the input molecular geometry – that could be obtained using quantum chemistry geometry optimization algorithms – should match the (main features of the) crystal structure. For instance, care should be taken when the optimized isolated molecule geometry adopts a different molecular conformation than in the crystal. This has been illustrated with the DAN case, showing that a change of conformation around the donor-π-acceptor system could attenuate the bond length alternation and thus lead to large underestimations of the molecular properties, and subsequently of the bulk properties.

The second aspect highlighted in this study is the role of electron correlation. The DFT is known to be very useful computational tool but sometimes it fails. This could be the case if more extended NLO chromophores are considered. Its performance should be confronted with the Hartree-Fock and MP2 methods. The latter method is currently the only one enabling the calculation of correlated wave-function results for large systems. Nevertheless, a drawback is the lack of the frequency dispersion description of the MP2 properties, which is here alleviated using the multiplicative scheme.

The third important aspect raised by this study is the impact of the chromophore electron density polarization due to surrounding molecules in the crystal lattice. This effect accounts for an enhancement of *ca.* 100-200% of the molecular first hyperpolarizability and thus influences strongly the calculated bulk $\chi^{(2)}$ tensor components. This factor is decisive in view of precise and reliable predictions of the bulk properties of new non-centrosymmetric phases on the basis of crystal structure parameters as the only empirical input parameter.

ACKNOWLEDGMENTS

This research was supported in part by PL-Grid Infrastructure as well as by the Belgium government (IUAP N° P7/05, Functional Supramolecular Systems). T.S. acknowledges the support from a Project operated within the Foundation for Polish Science MPD Programme co-financed by the EU European Regional Development Fund as well as the financial support of IUAP N° P7/05. The calculations were performed on the computing facilities of the Consortium des Équipements de Calcul Intensif (CÉCI), in particular those of the Plateforme Technologique de Calcul Intensif (PTCI) installed in the University of Namur, for which we gratefully acknowledge the financial support of the FNRS-FRFC (Conventions No. 2.4.617.07.F and 2.5020.11) and of the University of Namur.

REFERENCES

[1] Papadopoulos, M.G., Sadlej, A.J. and Leszczyński, J., [Non-linear Optical Properties of Matter – From Molecules to Condensed Phases], Springer, Dordrecht, (2006)

[2] Wong, M.S., Bosshard, Ch. and Günter, P, *Adv. Mater.*, **10**, 837–42 (2004).

[3] Champagne, B.; Bishop, D.M. *Adv. Phys. Chem.* **126**, 41-92 (2003).

[4] Whitten, A.E., Turner, P., Klooster, W.T., Piltz, R.O. and Spackman, M.A., *J. Phys. Chem. A* **110**, 8763-8776 (2006).

[5] Clark, R.D., Romero, A., Borbulevych, O.Ya., Antipin, M.Yu., Nesterov, V.N. and Timofeeva, T.V., *Acta Crystallogr., Sect. C-Cryst. Struct. Commun.* **56**, 336-338 (2000).

[6] Hurst, M. and Munn, R.W., *J. Mol. Electron.* **2**, 35-43 (1986)

[7] Reis, H., Papadopoulos, M.G., Hättig, C., Angyan, J.G. and Munn, R.W., *J. Chem. Phys.*, **112**, 14, 6161-6172 (2000)

[8] Reis, H., Papadopoulos, M.G., Calaminici, P., Jug , K. and Köster, A.M., *Chem. Phys.* **261**, 359-371 (2000)

[9] Gaussian 09, Revision D.1, Frisch, M.J.; Trucks, G.W.; Schlegel, H.B.; Scuseria, G.E.; Robb, M.A.; Cheeseman, J.R.; Scalmani, G.; Barone, V.; Mennucci, B.; Petersson, G.A.; Nakatsuji, H.; Caricato, M.; Li, X.; Hratchian, H.P.; Izmaylov, A.F.; Bloino, J.; Zheng, G.; Sonnenberg, J.L.; Hada, M.; Ehara, M.; Toyota, K.; Fukuda, R.; Hasegawa, J.; Ishida, M.; Nakajima, T.; Honda, Y.; Kitao, O.; Nakai, H.; Vreven, T.; Montgomery, Jr., J.A.; Peralta, J.E.; Ogliaro, F.; Bearpark, M.; Heyd, J.J.; Brothers, E.; Kudin, K.N.; Staroverov, V.N.; Kobayashi, R.; Normand, J.; Raghavachari, K.; Rendell, A.; Burant, J.C.; Iyengar, S.S.; Tomasi, J.; Cossi, M.; Rega, N.; Millam, J.M.; Klene, M.; Knox, J.E.; Cross, J.B.; Bakken, V.; Adamo, C.; Jaramillo, J.; Gomperts, R.; Stratmann, R.E.; Yazyev, O.; Austin, A.J.; Cammi, R.; Pomelli, C.; Ochterski, J.W.; Martin, R.L.; Morokuma, K.; Zakrzewski, V.G.; Voth, G.A.; Salvador, P.; Dannenberg, J.J.; Dapprich, S.; Daniels, A.D.; Farkas, Ö.; Foresman, J.B.; Ortiz, J.V.; Cioslowski, J.; Fox, D.J. Gaussian, Inc., Wallingford CT, (2009).

[10] Allen, F.H. and Bruno, I.J., *Acta cryst.. Sect. B,* **66**, 380–386 (2010).

[11] Grossman, C.H. and Garito, A.F., *Mol. Cryst. Liq. Cryst.*, **168**, 37–41 (2006).

[12] Lipscomb, G.F., Garito, A.F. and Narang, R.S., *Appl. Phys. Lett.*, **38**, 663-665 (1981).

[13] Morita, R., Kondo, T., and Kaneda, Y., *Jpn. J. Appl.*, **27**, L1131-L1133 (1988).

[14] Levine, B.F., Bethea, C.G., Thurmond, C.D., Lynch, R.T., and Bernstein, J.L., *J. Appl. Phys.*, **50**, 2523-2527 (1979).

[15] Bosshard, C., Gubler, U., Kaatz, P., Mazerant, W., and Meier, U. *Phys. Rev. B*, **61**(16), 10688–10701 (2000).

[16] Shoji, I., *J. Opt. Soc. Am. B*, **14**, 2268-2294 (1997).

[17] Hilger, A., Gisselbrecht, J.-P., Tykwinski, R.R., Boudon, C., Schreiber, M., Martin, R.E., Lüth, H.P., Gross, M. and Diederich, F., *Am. Chem. Soc.* **119**, 9, 2069-2078 (1997).

[18] Kerkoc, P., Zgonik, M., Sutter, K., Bosshard, Ch. and Günter, P., *J. Opt. Soc. Am. B* **7**, 313-319 (1990).